COMMUNICATION

ChemComm
www.rsc.org/chemcomm

Crystallography and magnetism of radicals with hindered hydroxyl groups: 2-(3,5-di-*tert*-butyl-4-hydroxyphenyl)-4,4,5,5-tetramethyl-4,5-dihydro-1*H*-imidazole-3-oxide-1-oxyl and 2-(3,5-di-*tert*-butyl-4-hydroxyphenyl)-4,4,5,5-tetramethyl-4,5-dihydro-1*H*-imidazole-1-oxyl†

Patrick Taylor and Paul M. Lahti*
Department of Chemistry, University of Massachusetts, Amherst, MA 01003, USA.
E-mail: lahti@chem.umass.edu

Received (in Corvallis, OR, USA) 5th August 2004, Accepted 17th September 2004
First published as an Advance Article on the web 27th October 2004

Radicals 1–2 form networks of OH···ON and OH···Me(nitroxide) interactions. In 2, a frustrated network forms with insufficient N–O units to form extended chain interactions. The magnetism of 1 fits a 1-D Heisenberg model with $J/k = -25$ J mol^{-1}, while 2 shows more complex exchange behaviour consistent with its disordered crystal lattice.

Hydrogen bonds play important roles as crystallographic scaffolding and electronic exchange elements in molecular magnetic materials.[1] As part of our studies of hydrogen bonding in organic magnetic systems, we have carried out crystallographic and magnetic analyses of 2-(3,5-di-*tert*-butyl-4-hydroxyphenyl)-4,4,5,5-tetramethyl-4,5-dihydro-1*H*-imidazole-3-oxide-1-oxyl (**1**) and 2-(3,5-di-*tert*-butyl-4-hydroxyphenyl)-4,4,5,5-tetramethyl-4,5-dihydro-1*H*-imidazole-3-oxide-1-oxyl (**2**). Radical **1** has previously been mentioned in reports limited to descriptions of its ESR and UV-vis spectra, as well as its oxidation chemistry.[2] To our knowledge there are no magnetocrystallographic studies of **1**,

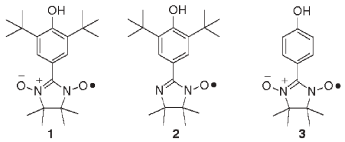

and no studies at all of **2**. But, Veciana and coworkers extensively studied[3] related radical **3**, which exhibits ferromagnetic exchange interactions at reduced temperatures. These studies aimed to interpret magnetic behaviour based on interatomic contacts between the nitroxide NO units and the phenolic OH, as well as other contacts. We were analogously interested in effects of the sterically hindering *tert*-butyl substituents upon the crystallography and magnetism of **1–2** by comparison to **3**.

Radical **1** was synthesized by condensation of 2,3-bis(hydroxylamino)-2,3-dimethylbutane hydrogensulfate[4] with 3,5-di-*tert*-butyl-4-hydroxybenzaldehyde, followed by oxidation using aqueous $NaIO_4$ to give a stable azure solid. Treatment of **1** with $NaNO_2$ in dichloromethane with catalytic acid by the method of Ullman *et al.*[5] yielded modest amounts of **2** as a brick-red solid after careful column chromatography. Radical **2** is less stable in solution and tends to decompose, but appears stable for months once isolated in the solid state. The room temperature ESR spectrum of **1** in toluene shows a 1 : 3 : 5 : 3 : 1 five-line hyperfine splitting pattern consistent with two equivalent nitrogens having $a_N = 7.6$ G. The spectrum for **2** shows a 1 : 1 : 2 : 1 : 2 : 1 : 1 seven-line pattern consistent with two inequivalent nitrogens having $a_N = 9.33$ and 4.1 G. Both spectra are readily simulated, as shown in the ESI.† Both compounds were characterized‡ by crystallography, spectroscopy, and magnetic measurements.

† Electronic supplementary information (ESI) available: synthetic details for **1–2**; FTIR, ESR, crystallographic, computational summaries. See http://www.rsc.org/suppdata/cc/b4/b411574k/

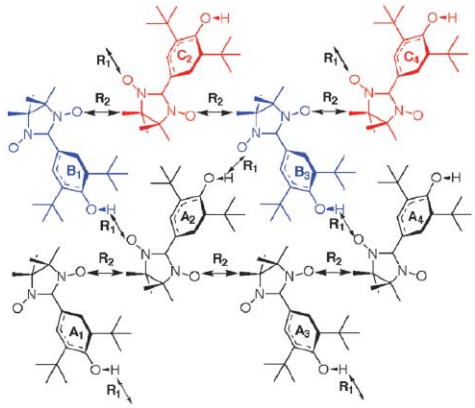

Fig. 1 Close contacts in **1**. Labels A, B, C and different colouration represent crystallographically distinct molecules. R_1 is a OH···O(N) contact, R_2 is a (N)O···Me(nitroxide) contact.

Single crystal X-ray diffraction analysis of **1** showed an array of OH···O(N) and (N)O···Me(nitroxide) 1-D chains forming a 3-D network throughout the lattice. These contacts are shown as R_1 and R_2 in Fig. 1, respectively. There are three slightly different molecules of **1** in the unit cell differing mainly in their interannular torsion angles (phenyl to nitronylnitroxide torsion within the range 30.8–34.9°) forming two distinguishable zig-zag chains of R_1 contacts—B_1–A_2–B_3–A_4 and A_1–C_2–A_3–C_4 in the figure—but the chains are extremely similar in relative geometry, so there is effectively only one type of 1-D OH···O(N) contact chain based on R_1. These contacts are non-collinear with ∠O–H···O ~ 134–136° and r(H···O) = R_1 ~ 2.2–2.3 Å, depending upon crystallographic placement of the hydrogen atom and which of the three distinct molecules is considered. Table 1 summarizes various molecular interatomic structural parameters in **1** for comparison with **2** and **3**.

Table 1 Selected structure and crystal packing parameters

	Molecular parameters	Intermolecular contacts
1	rNO = 1.275–1.298 Å	rO(H)···O(N) = 2.880–2.945 Å
	rCN = 1.327–1.352	r(O)H···O(N) = 2.25–2.30
	Transannular rCC = 1.450–1.453	r(N)O···C(H$_3$) = 3.271–3.429
	Interannular torsion = 30.8–33.8°	
2	rNO = 1.275–1.289 Å	rO(H)···O(N) = 2.936–2.981 Å
	rC–N = 1.327–1.352	r(O)H···O(N) = 2.19–2.20
	rC=N = 1.278–1.308	r(N)O···C(H$_3$) = 2.930–3.774
	Transannular rCC = 1.447–1.489	
	Interannular torsion = 24.9–32.4°	
3[b]	rNO = 1.274–1.298 Å	rO(H)···O(N) = 2.674–2.690 Å
	rCN = 1.331–1.363	r(O)H···O(N) = 1.61–1.66
	Transannular rCC = 1.444–1.452	r(N)O···C(H$_3$) = 3.354–3.505
	Interannular torsion = 30-0–33.2°	

[a] See ESI for details of individual parameters and distances. [b] Ref. 3a

DOI: 10.1039/b411574k

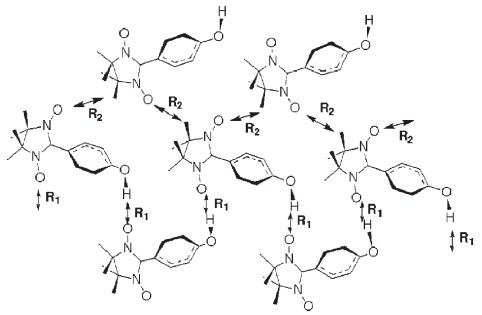

Fig. 2 Close contacts in **3**. R_1 is a OH···O(N) contact, R_2 is a (N)O···Me(nitroxide) contact. All molecules are structurally the same due to the point group symmetry (ref. 3*a*).

We compared the interatomic contacts in **1** to those analogous in **3** (Fig. 2). Structurally, the molecules are similar. The packing is a bit simpler in **3** (only one symmetrically distinct molecule). The (N)O···Me(nitroxide) contacts R_2 are relatively similar to those in **1** (Table 1), although it is difficult to represent this clearly in the comparison of Figs. 1 and 2. By contrast, the close interatomic distances R_1 are comprised of nearly collinear OH···O(N) contacts that are significantly shorter ($R_1 \sim 1.6$ Å) than in **1** (or **2**).[3a] The difference is surely influenced by the steric hindrance in **1** which does not permit really close OH to O(N) approaches. Interestingly, the FTIR spectra of **1–2** show broadened OH stretching bands at 3440–3480 cm^{-1} (see ESI†), unlike 2,6-di-*t*-butylphenols that lack hydrogen bonding, so we feel that the OH···O(N) contacts in **1–2** can still reasonably be classified as weak hydrogen bonds, and not just dipolar contacts.

The molecular structure of **2** is similar to that of **1**. It exhibits OH···O(N) contacts similar in length and geometry to those in **1** (Fig. 3, Table 1). It also has some (N)O···Me(nitroxide) contacts with similar lengths. But, in terms of 3-D OH···O(N) and OH···Me(nitroxide) chain formation, **2** is crystallographically "frustrated" and defective. The packing of **2** is quite similar to that of **1**, as shown in Fig. 2, but is disordered even at 100 K. There are three crystallographically distinct molecules in the lattice, one of which exhibits a 65 : 35 positional disorder of the NO group interchanged with the imidazole nitrogen (:N), and another of which exhibits the same ON/:N disorder plus a torsional disorder of the iminoylnitroxide unit *vs.* the phenolic ring (24.5 and 143.2°) to produce four different oxygen positions. Due to the disorder, throughout the lattice of **2**, sites that in **1** have an ON group have instead an imidazole :N. Despite the similarity of molecular packing between **1** and **2**, a full 3-D network of OH···O(N) and OH···Me(nitroxide) contacts in **2** is impossible. As a result, unlike

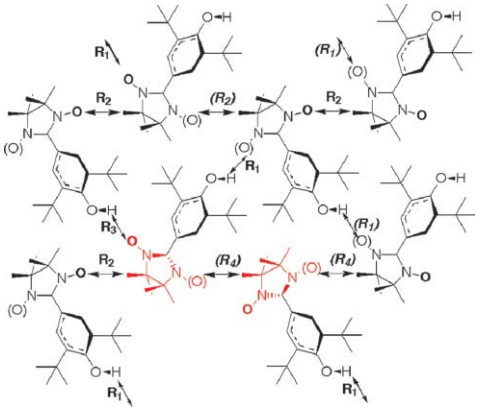

Fig. 3 Close contacts in **2**. R_1 and R_3 are OH···O(N) contacts, R_3 and R_4 are (N)O···Me(nitroxide) contacts. Oxygen atoms in parentheses indicate alternate crystallographic positions. Contacts in parentheses indicate a contact only for alternate crystallographic positions. Red-coloured moiety indicates alternate torsional form in the lattice.

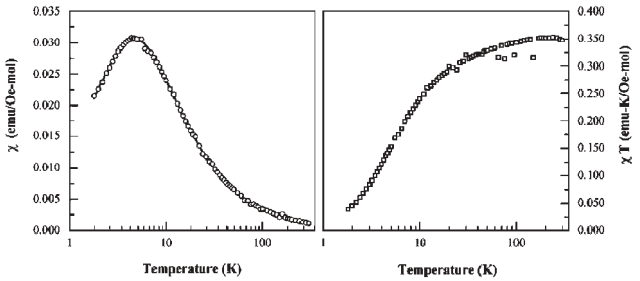

Fig. 4 χ *vs.* T and χT *vs.* T plots for **1** at 1000 Oe. The solid line in the left hand plot shows the fit to eqn. (1).

1, **2** has a variety of very different intermolecular contacts, complicating its magnetostructural analysis.

Figs. 4 and 5 show the variable temperature dc magnetic susceptibility behaviours of **1** and **2** as polycrystalline samples at 1000 Oe, after temperature independent corrections. At higher temperatures, χT should reach a limiting value of ~0.37 emu K Oe^{-1} mol^{-1} for $S = 1/2$ spin carriers. This is observed. The downturn at lower temperatures of $\chi T(T)$ shows the presence of intermolecular antiferromagnetic (AFM) exchange interactions. Compound **1** shows monotonic behaviour of χT *vs.* T, while **2** shows steps consistent with multiple exchange mechanisms due to the disordered crystal lattice.

We fitted the $\chi(T)$ data of **1** to a 1-D Heisenberg chain model[6] with mean-field and paramagnetic contributions, eqn. (1). Since $\chi(T)$ actually turns down at lower temperatures, this fit is more sensitive than a χT *vs.* T fit for this case. For eqn. (1), the coefficients A–F are given in various references, J is the intermolecular exchange constant, P is the fraction of paramagnetic spins, N is Avogadro's number, g the Lande constant, k the Boltzmann constant, S the spin quantum number, and β the Bohr magneton constant. We found an excellent fit (Fig. 4) where $J/k = -3.0$ K $= -25.1$ J mol^{-1}, and an averaged mean field interaction of $\theta = -0.38$ K; the fitted paramagnetic component of isolated, non-interacting spins was 2.2%.

$$\chi = (1-P)\left(\frac{4C_0}{[T-\theta]}\right)\frac{A+Bx+Cx^2}{1+Dx+Ex^2+Fx^3} - P\frac{0.375}{T}$$
$$x = |J/kT|;\ C_0 = Ng^2\beta^2S(S+1)/3k \qquad (1)$$

The low temperature behaviour of **2** does not tend to $\chi = 0$, suggesting the presence of short chain interactions and/or isolated spins as well as spin pairing interactions. Various models did not give a good fit for the magnetic behaviour over the full temperature range. However, we found a good fit to the $\chi T(T)$ data for $T <$ 50 K using a double Bleaney–Bowers[7] model, eqn. (2). Here we used two spin pairing exchange constants J_1/k and J_2/k, assumed contributions only from two spin pairing mechanisms (fractions P and $[1 - P]$), and the same definitions of constants used for eqn. 1. The fit (Fig. 5) gives $J_1/k = -0.45$ K $= -3.8$ J mol^{-1} ($P = 65\%$ of pairs), $J_2/k = -10$ K $= -83$ J mol^{-1} (35% of pairs). While the real behaviour is likely to be more complex than this model implies, we felt that spin pairing behaviour should dominate at lower temperatures, and that there would be at least two types of pairing, given the disordered crystal structure of **2**. The observed

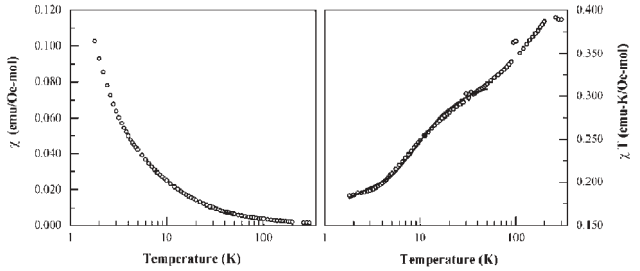

Fig. 5 χ *vs.* T and χT *vs.* T plots for **2** at 1000 Oe. The solid line in the right hand plot shows the fit to eqn. (2) for $T < 50$ K.

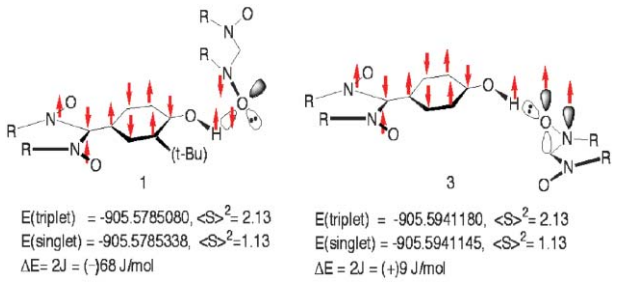

Scheme 1 UB3LYP/6-31G* energies, $<S^2>$ expectation values, and qualitative spin distribution for model dyads of **1** and **3** (R = H in the computations). No ZPE corrections were applied.

behaviour is consistent with this.

$$\chi = (1-P)\left(\frac{2C_0}{T}\right)\frac{2e^x}{1+3e^x} - P\left(\frac{2C_0}{T}\right)\frac{2e^y}{1+3e^y}$$
$$x = |J_1/kT|; y = |J_2/kT|; C_0 = 0.375g^2/4 \quad (2)$$

The qualitative difference between the magnetic behaviours of **1–2** (AFM exchange) by comparison to **3** (FM chain formation) is notable. The crystallographic packing motifs are similar, save for difference in the OH···O(N) contacts described above. We suggest that the difference in the OH···O(N) contacts is a major contributor to the different behaviours. In **1**, the contact geometry requires that OH overlaps with a nitroxide π-SOMO, not with a nitroxide σ-lone-pair. This is consistent with the longer OH···O(N) distance in **1** by comparison[3a] to **3**, since the latter can achieve a stronger hydrogen bonding interaction involving the nitroxide lone-pair orbital due to its more typical, linear OH···ON contact. We computed the triplet to singlet splitting of **1** at the UB3LYP/6-31G* level with Gaussian03[8] for a dimer model incorporating the OH···ON contact having the crystallographic geometry found in **1**, replacing the *tert*-butyl groups and tetramethylethano bridges in the radical groups with C–H bonds. Singlet state computations were done using a broken symmetry wavefunction, similar to methodology described elsewhere.[9]

Scheme 1 summarizes the computations. The OH···O(N) contact in **1** yields a singlet (AFM preference), while the contact in **3** yields a triplet (FM preference), in accord with experimental exchange behaviours. Overly emphatic comparison of the computed to the experimental exchange values should be viewed with caution. The experimental exchange analysis for **1** uses a 1-D chain model, and the computational model simple dyads. In addition, the computed splittings are small given the uncertainties of broken symmetry singlet state computations with hybrid density functionals. Finally, given the complexity of ascribing[1b] magnetic behaviour in organic radicals to specific structural features, we must note that other contacts in the systems might contribute to the overall magnetism, such as the (N)O···Me(nitroxide) contacts. Still, this level of theory has frequently[9] been used to analyze radical–radical interactions, and our computations give appropriate qualitative agreement with the observed exchange behaviour. Because other crystallographic contacts in **1** are similar to those found in **3**, we feel that the mechanism of Scheme 1 is likely to be a major contributor to the qualitative reversal of exchange behaviour from FM to AFM in **3** *vs.* **1**, as the computations support.

Overall, **1–3** exemplify the fascinatingly subtle effects of crystal structure upon magnetic behaviour in organic radicals. The major qualitative change in behaviour from **1–2** to **3** is consistent with the change in OH···O(N) contacts due to the sterics of the *tert*-butylated compounds. Although hydrogen bonding is a useful means to organize crystal scaffolding, its electronic effect on bulk magnetic and exchange behaviour is not always straightforward to predict. Hopefully, further study of such systems will continue to help clarify such magnetostructural relationships.

This work was supported by the National Science Foundation (NSF CHE-0109094, CHE-0415716, and CTS-0116498). We thank Dr. A. Chandrasekaran of the UMass-Amherst X-ray Structural Characterization Center (NSF CHE-9974648) for crystallographic analyses, and Dr. G. Dabkowski for elemental analyses. PML thanks Prof. Juan Novoa for helpful discussions.

Notes and references

‡ For **1**; mp 184–185 °C. Anal. calcd for $C_{21}H_{33}N_2O_3$: C 69.77, H 9.20, N 7.75; found: C 69.83; H 9.16; N 20.49. ESR (9.656 GHz, toluene): a_N = 7.55 G (2 N). FTIR (KBr, cm^{-1}): 3443 (broad, OH), 2968 (CH stretch). Crystallography: deep blue needle from dichloromethane, 0.35 × 0.35 × 0.20 mm, formula = $C_{21}H_{33}N_2O_3$, M = 361.49, monoclinic, space group $P2_1/c$, T = 293 K, Z = 12, a = 17.3092(2), b = 30.9285(3), c = 12.1652(1) Å, β = 90.8163(5)°, V = 6511.95(11) Å^3, D_{calc} = 1.106 g cm^{-3}, λ(Mo–Kα) = 0.7107 Å, μ = 0.073 mm^{-1}, F(000) = 2364. 21763 reflections were recorded at a threshold intensity of $2\sigma(I)$. 11406 independent reflections (R_{int} = 0.0406) were analyzed with 705 parameters using SHELXL-97. For 6818 reflections with $I > 2\sigma(I)$) $R(I > 2\sigma)$ = 0.0779, $wR(I > 2\sigma)$ = 0.2039; R(all) = 0.1279, wR(all) = 0.2281, goodness of fit on F^2 = 1.358. CCDC 243200. For **2**, mp 190–192 °C. Anal. calcd for $C_{21}H_{33}N_2O_2$: C 73.00, H 9.63, N 8.11; found: C 72.92; H 9.55; N 7.83. ESR (9.652 GHz, toluene): a_N = 9.33, 4.14 G. FTIR (KBr, cm^{-1}): 3474 (broad, OH), 2969 (CH stretch). Crystallography: red needle from hexane–ethyl aceteate, 0.70 × 0.50 × 0.15 mm, formula = $C_{21}H_{33}N_2O_2$, M = 345.49, orthorhombic, space group $P2_12_12_1$, T = 173 K, Z = 12, a = 111.8548(1), b = 17.1035(2), c = 30.8698(4) Å, V = 625912(12) Å^3, D_{calc} = 1.100 g cm^{-3}, λ(Mo–Kα) = 0.7107 Å, μ = 0.070 mm^{-1}, F(000) = 2268. 10723 reflections were recorded at a threshold intensity of $2\sigma(I)$. 10723 independent reflections (R_{int} = 0.000) were analyzed with 705 parameters using SHELXL-97. For 7222 reflections with $I > 2\sigma(I)$) $R(I > 2\sigma)$ = 0.0680, $wR(I > 2\sigma)$ = 0.1579; R(all) = 0.1122, wR(all) = 0.1834, goodness of fit on F^2 = 1.032. An absolute structure parameter of 0(3) was used. CCDC 243201. See http://www.rsc.org/suppdata/cc/b4/b411574k/ for crystallographic data in .cif or other electronic format.

1 (*a*) J. Cirujeda, E. Hernandez-Gasio, F. Lanfranc de Panthou, J. Laugier, M. Mas, E. Molins, C. Rovira, J. J. Novoa, P. Rey and J. Veciana, *Mol. Cryst. Liq. Cryst. Sci. Technol., Sect. A*, 1995, **271**, 1; (*b*) J. Veciana, J. Cirujeda, J. J. Novoa and M. Deumal, in *Magnetic Properties of Organic Materials*, ed. P. M. Lahti, New York, NY, 1999, p. 573.
2 (*a*) L. Y. Chiang, R. B. Upasani and J. W. Swirczewski, *Mater. Res. Soc. Symp. Proc.*, 1992, **247**, 435; (*b*) K. Ishiguro, M. Ozaki, N. Sekine and Y. Sawaki, *J. Am. Chem. Soc.*, 1997, **119**, 3625; (*c*) K. Ishiguro, M. Ozaki, Y. Kamekura, N. Sekine and Y. Sawaki, *Mol. Cryst. Liq. Cryst. Sci. Technol., Sect. A*, 1997, **306**, 75.
3 (*a*) E. Hernandez, M. Mas, E. Molins, C. Rovira and J. Veciana, *Angew. Chem., Int. Ed. Engl.*, 1993, **32**, 882; (*b*) J. Cirujeda, J. Vidal-Gancedo, O. Juergens, F. Mota, J. J. Novoa, C. Rovira and J. Veciana, *J. Am. Chem. Soc.*, 2000, **122**, 11393.
4 V. Ovcharenko, S. Fokin and P. Rey, *Mol. Cryst. Liq. Cryst. Sci. Technol., Sect. A*, 1999, **334**, 109.
5 E. F. Ullman, L. Call and J. H. Osiecki, *J. Org. Chem.*, 1970, **35**, 3623.
6 J. C. Bonner and M. E. Fisher, *Phys. Rev. A*, 1964, **135**, 650; J. C. Bonner, Ph.D. Dissertation, University of London, UK, 1968.
7 B. Bleaney and K. D. Bowers, *Proc. R. Soc. London, Ser. A*, 1952, 214.
8 (*a*) A. D. Becke, *Phys. Rev. A*, 1988, **38**, 3098; (*b*) C. Lee, W. Yang and R. G. Parr, *Phys. Rev. B*, 1988, **37**, 785; (*c*) For Gaussian03, see: M. J. Frisch, G. W. Trucks, H. B. Schlegel, G. E. Scuseria, M. A. Robb, J. R. Cheeseman, J. A. J. Montgomery, T. Vreven, K. N. Kudin, J. C. Burant, J. M. Millam, S. S. Iyengar, J. Tomasi, V. Barone, B. Mennucci, M. Cossi, G. Scalmani, N. Rega, G. A. Petersson, H. Nakatsuji, M. Hada, M. Ehara, K. Toyota, R. Fukuda, J. Hasegawa, M. Ishida, T. Nakajima, Y. Honda, O. Kitao, H. Nakai, M. Klene, X. Li, J. E. Knox, H. P. Hratchian, J. B. Cross, C. Adamo, J. Jaramillo, R. Gomperts, R. E. Stratmann, O. Yazyev, A. J. Austin, R. Cammi, C. Pomelli, J. W. Ochterski, P. Y. Ayala, K. Morokuma, G. A. Voth, P. Salvador, J. J. Dannenberg, V. G. Zakrzewski, S. Dapprich, A. D. Daniels, M. C. Strain, O. Farkas, D. K. Malick, A. D. Rabuck, K. Raghavachari, J. B. Foresman, J. V. Ortiz, Q. Cui, A. G. Baboul, S. Clifford, J. Cioslowski, B. B. Stefanov, G. Liu, A. Liashenko, P. Piskorz, I. Komaromi, R. L. Martin, D. J. Fox, T. Keith, M. A. Al-Laham, C. Y. Peng, A. Nanayakkara, M. Challacombe, P. M. W. Gill, B. Johnson, W. Chen, M. W. Wong, C. Gonzalez and J. A. Pople, in *Gaussian 03, Revision B.03*, Pittsburgh, PA, 2003.
9 For recent examples, see: (*a*) Y. Takano, T. Taniguchi, H. Isobe, T. Kubo, Y. Morita, K. Yamamoto, K. Nakasuji, T. Takui and K. Yamaguchi, *J. Am. Chem. Soc.*, 2002, **124**, 11122; (*b*) G. D. McManus, J. M. Rawson, N. Feeder, J. van Duijn, E. J. L. McInnes, J. J. Novoa, R. Burriel, F. Palacio and P. Oliete, *J. Mater. Chem.*, 2001, **11**, 1992.